<u>Synoptic Meteorology II: Self-Development in the IPV Framework</u>

In this week's lecture, we described the self-development of an upper-tropospheric trough and accompanying surface cyclone in the IPV framework from an idealized perspective. Here, we wish to extend this framework to a real-world example. We leverage GFS numerical model forecasts plotted by [Tropical Tidbits]() and [Alicia Bentley]() for this illustration.

Our case of interest is a midlatitude cyclone that was forecast to develop, mature, and occlude over the central United States between 1200 UTC 26 February and 1800 UTC 27 February 2023. Three sets of images are provided:

- 330-K isentropic potential vorticity (color shading every 0.4 PVU), pressure (grey contours every 50 hPa), and horizontal wind (half-barb: 5 kt, barb: 10 kt, pennant: 50 kt), plus 850 hPa relative vorticity (purple contours, with the contour interval unstated).
- 850 hPa geopotential height (black contours every 30 m or 3 dam), equivalent potential temperature (color shading every 6 K), and horizontal wind (half-barb: 5 kt, barb: 10 kt, pennant: 50 kt).
- 300-200 hPa layer-mean potential vorticity (grey contours every 1 PVU), 300-200 hPa layer-mean divergent component of the wind (black vectors, with the reference vector given in the lower-right corner of each image), 600-400 hPa layer-mean ascent (red contours every $5x10^{-3}$ hPa s^{-1}), 250 hPa wind speed (shaded in cool colors in m s^{-1}), and column-integrated precipitable water (shaded in warm colors in mm).

The first two image sets document the upper- and lower-tropospheric evolution of the combined trough-cyclone system, whereas the last image set provides a measure of diabatic forcing on the upper-tropospheric pattern. We will first focus on the first two image sets, then use the third image set to document how the combined trough-cyclone evolution is influenced by diabatic processes.

The first three forecast times, corresponding to the 72-, 78-, and 84-h forecasts, document initial surface cyclone development. An intense, neutrally tilted cyclonic IPV maximum partially cutoff from the large-scale flow propagates eastward through the Intermountain West (Figs. 1-3). As it approaches the Front Range of the Rocky Mountains, a surface cyclone with minimum sea-level pressure of 987 hPa (Fig. 3) develops over the central Great Plains. This cyclone develops along a pre-existing baroclinic zone characterized by contours of constant 850 hPa equivalent potential temperature oriented from southwest to northeast across the south-central United States (Figs. 7-8), with the cyclone's development concurrently occurring with the development of associated cold and warm fronts (Fig. 9).

Over the subsequent three forecast times, corresponding to the 90-, 96-, and 102-h forecasts, the cyclonic IPV maximum intensifies and becomes increasingly negatively tilted (Figs. 4-6). This occurs as the downstream ridge (associated with a negative IPV anomaly) builds poleward and northwestward, including to the north of the cyclonic IPV maximum (Figs. 4-6). The rearward tilt from the surface cyclone to the cyclonic IPV maximum decreases during this time, with the two ultimately becoming vertically aligned with each other in the 96-102 h forecasts (Figs. 5-6). This corresponds to the surface cyclone intensifying from 987 hPa in the 84-h forecast to 973 hPa in the 102-h forecast (Figs. 3, 6). Likewise, the surface cyclone's fronts become better defined during the 84-96 h forecast period (Figs. 9-11), with the surface cyclone ultimately becoming secluded within relatively warm and moist lower-tropospheric air (Fig. 12) as it becomes vertically stacked with the upper-tropospheric cyclonic IPV maximum (Fig. 6).

The role of diabatic processes in the trough-cyclone evolution is highlighted by Figs. 13-18. Large midtropospheric ascent and upper-tropospheric divergence develop ahead of the cyclonic IPV maximum – and nearly coincident with the surface cyclone – by the 96-h forecast (Fig. 16). Such large ascent and upper-tropospheric divergence are presumably associated with diabatic warming in deep, moist convection. The upper-tropospheric divergence results in negative potential-vorticity advection, characterized by flow across the upper-tropospheric potential-vorticity contours from low toward high values, northeastward of the cyclonic IPV maximum (Figs. 16-18). This helps to facilitate the amplification of the downstream ridge from poleward of the cyclonic IPV maximum – helping the cyclonic IPV maximum to acquire a negative tilt – to the northeast of the cyclonic IPV maximum; it also helps to facilitate the amplification of the associated upper-tropospheric jet (Figs. 16-18).

The evolution described herein is consistent with self-development from an IPV perspective. Were we to consider this same case from the quasi-geostrophic perspective, the same insight would be obtained. However, it is arguably somewhat easier to see the contributions of diabatic heating to the trough-cyclone evolution in the IPV framework, representing one advantage over the quasi-geostrophic Pettersen-Sutcliffe development framework.

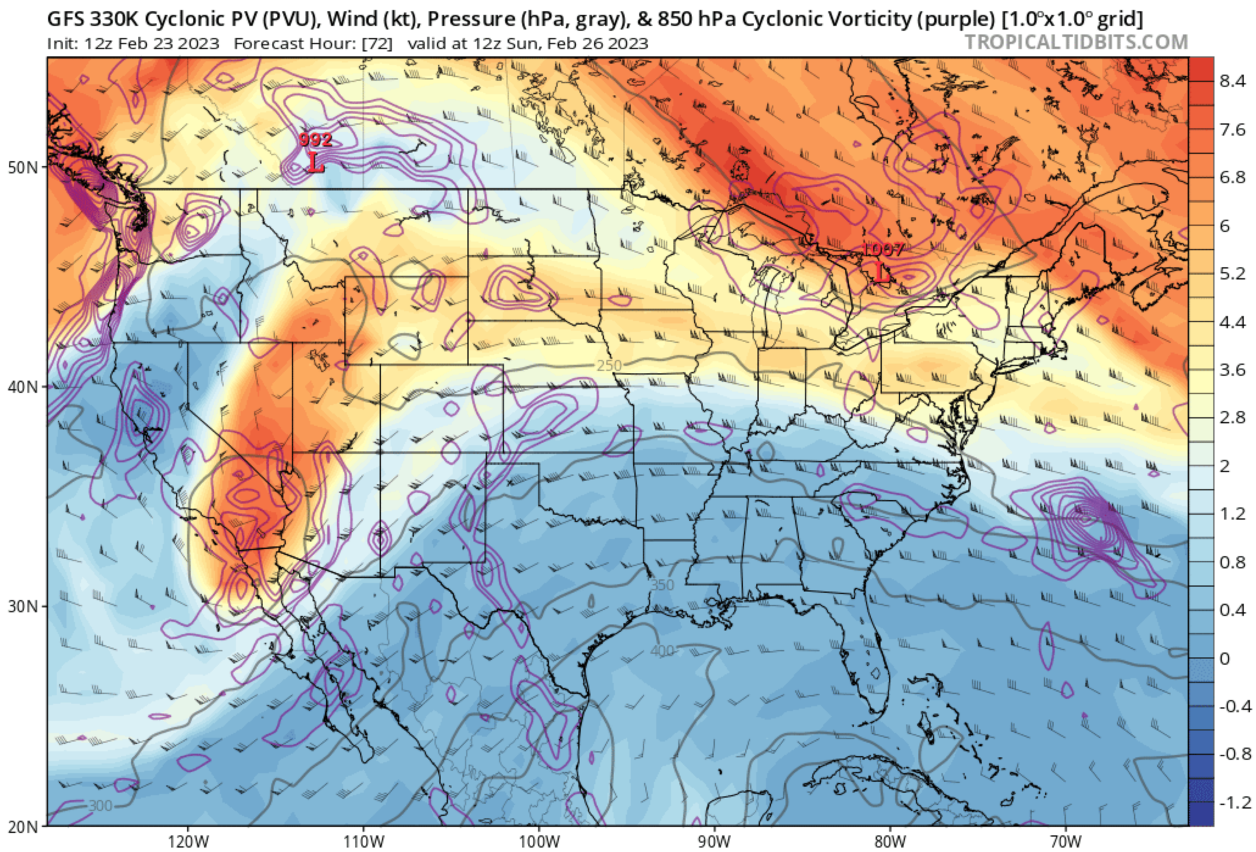

Figure 1. GFS 72-h forecast (valid 1200 UTC 26 February 2023) of 330-K potential vorticity (shaded in PVU per the color bar at right), pressure (grey contours in hPa), and wind (half-barb: 5 kt, full barb: 10 kt, pennant: 50 kt); 850 hPa cyclonic vorticity (purple contours); and cyclonic sea-level pressure anomalies (red markers). Figure obtained from Tropical Tidbits.

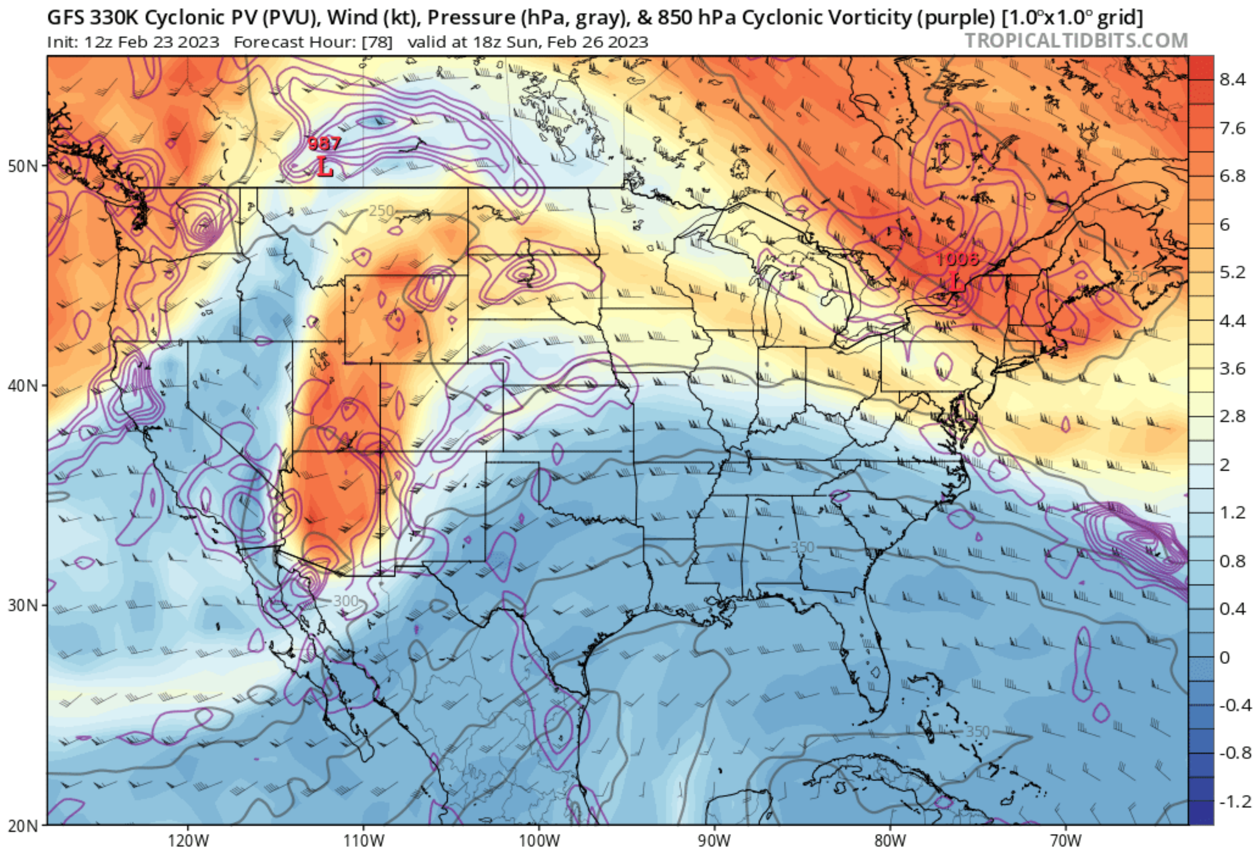

Figure 2: As in Fig. 1, except the 78-h forecast valid at 1800 UTC 26 February 2023.

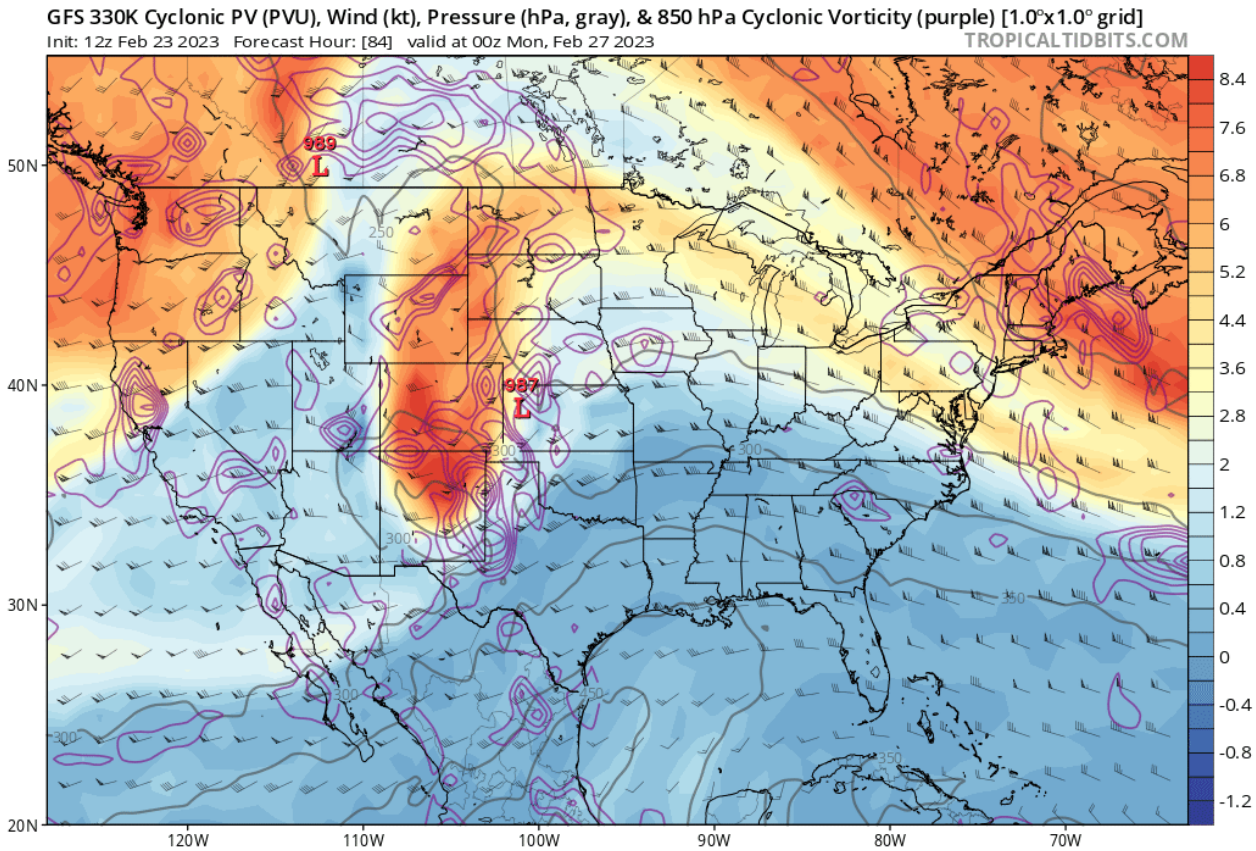

Figure 3: As in Fig. 1, except the 84-h forecast valid at 0000 UTC 27 February 2023.

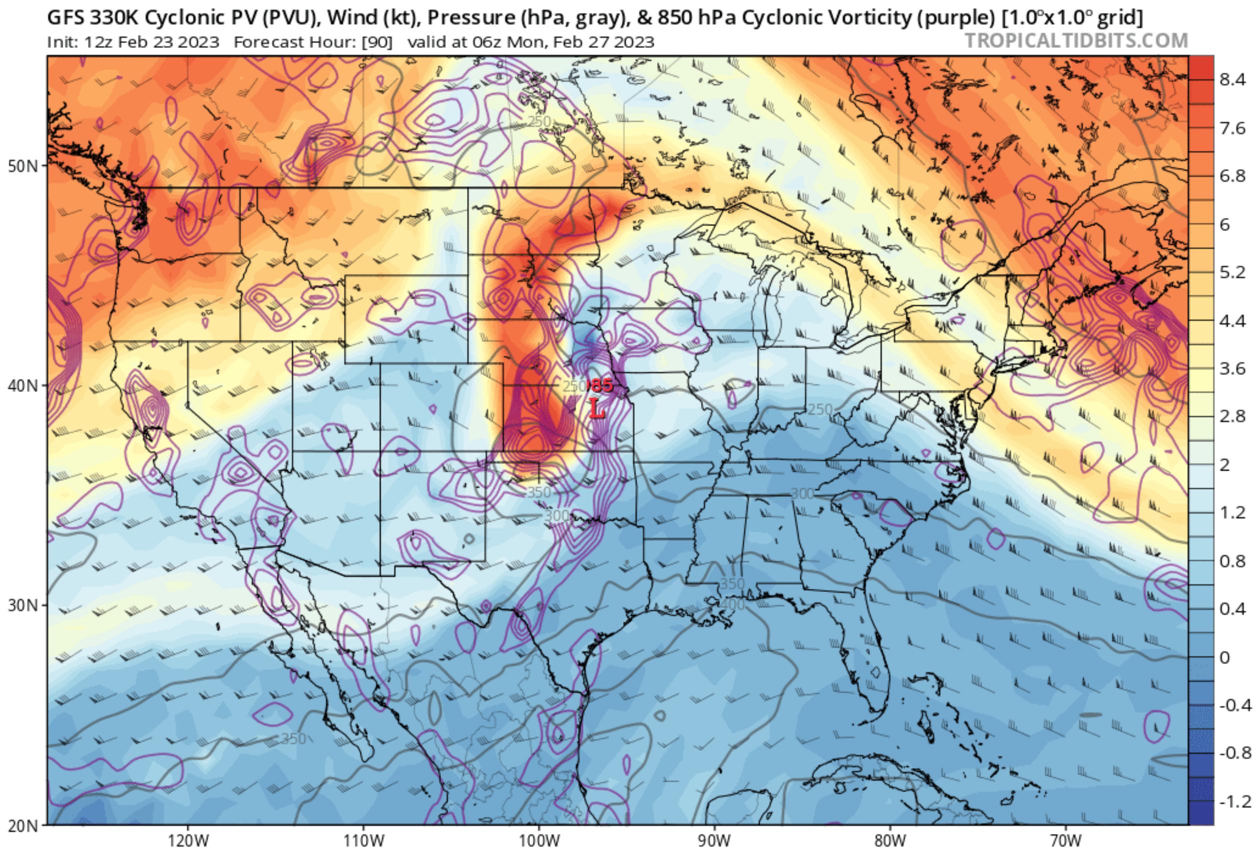

Figure 4: As in Fig. 1, except the 90-h forecast valid at 0600 UTC 27 February 2023.

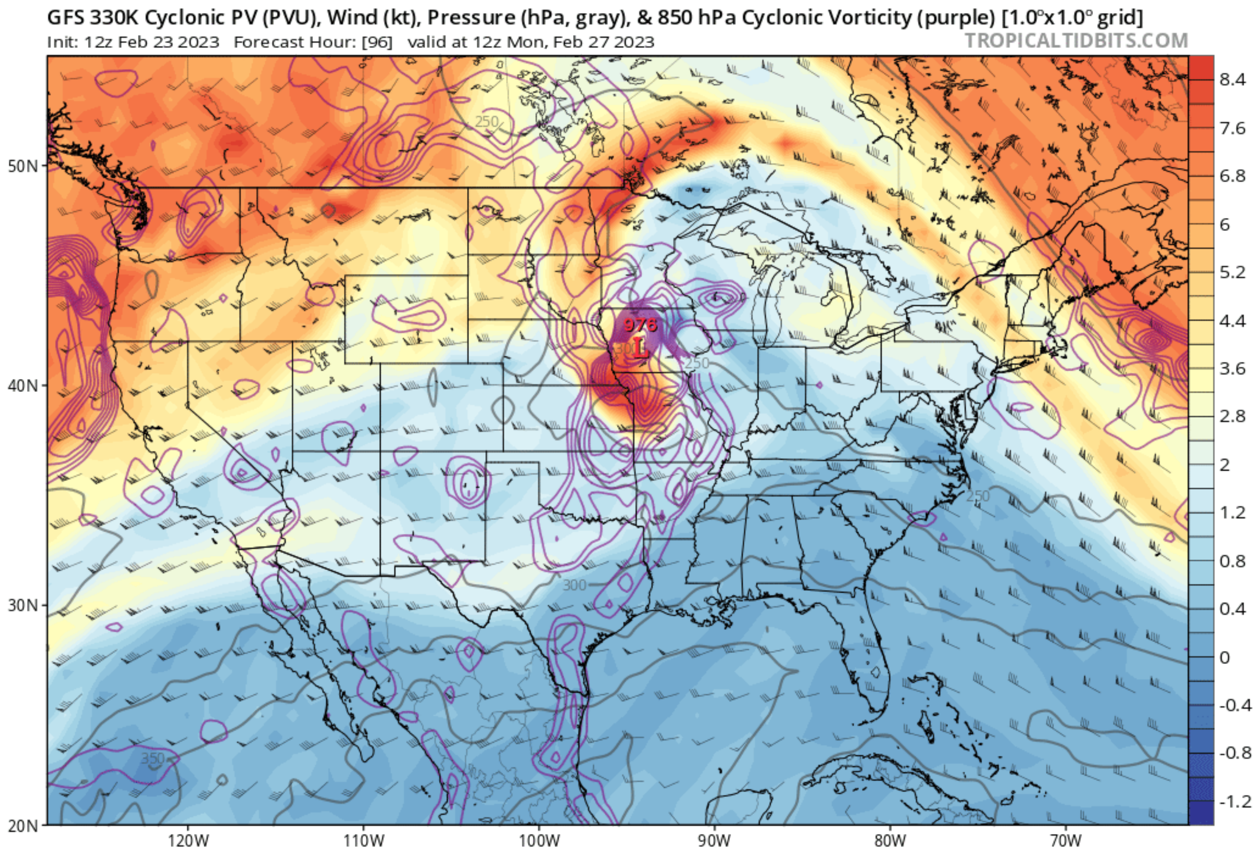

Figure 5: As in Fig. 1, except the 96-h forecast valid at 1200 UTC 27 February 2023.

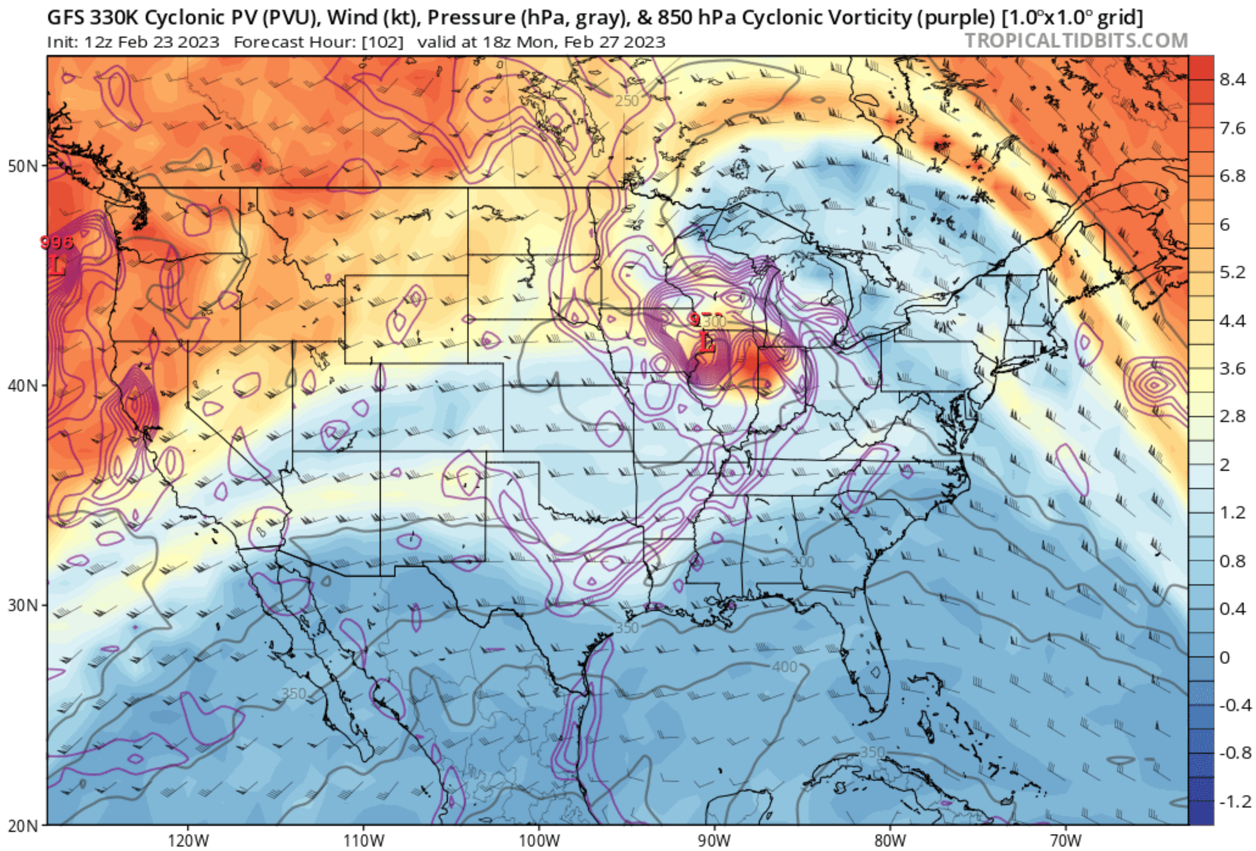

Figure 6: As in Fig. 1, except the 102-h forecast valid at 1800 UTC 27 February 2023.

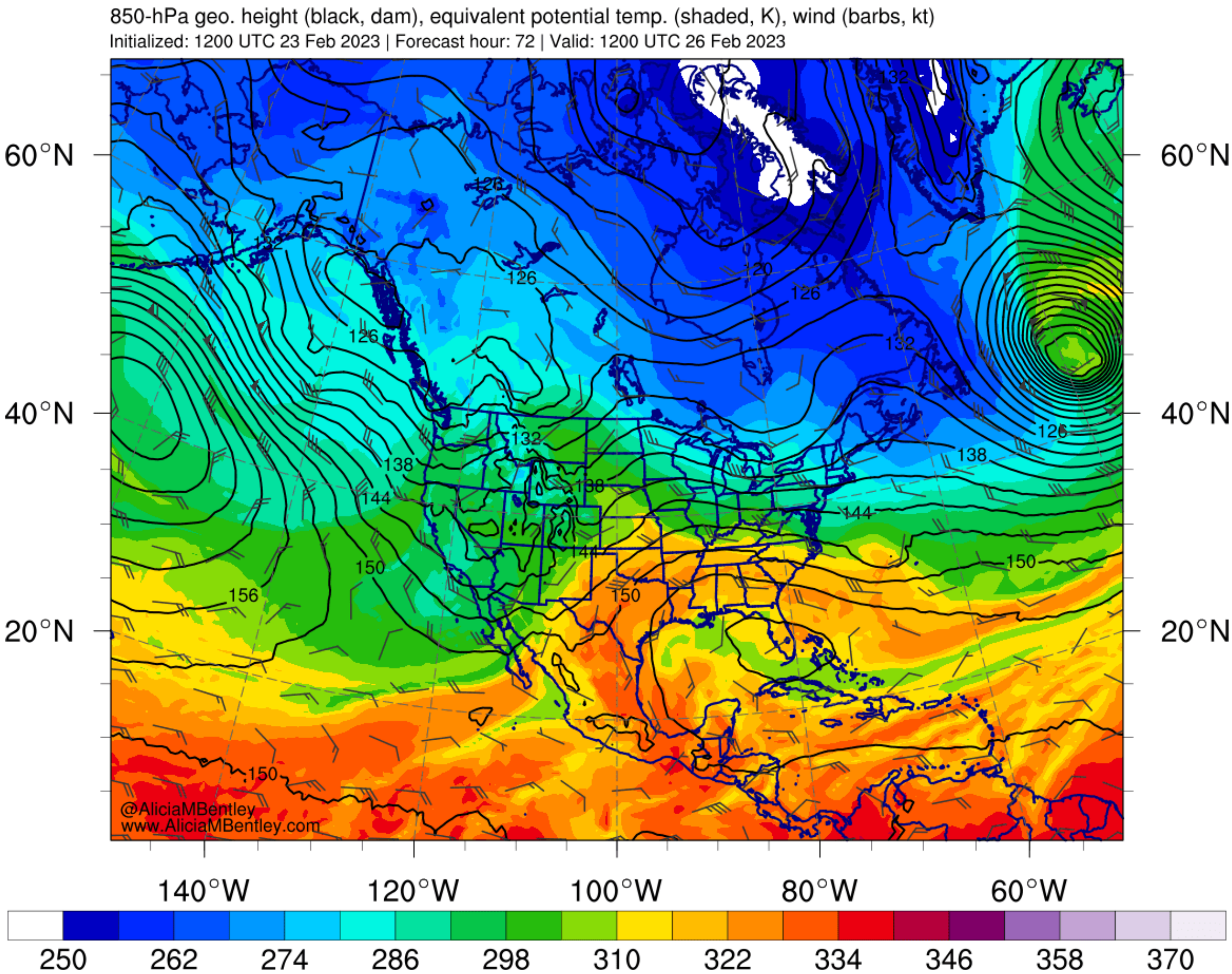

Figure 7: GFS 72-h forecast 850 hPa geopotential height (black contours every 30 m or 3 dam), equivalent potential temperature (color shading every 6 K), and horizontal wind (half-barb: 5 kt, barb: 10 kt, pennant: 50 kt). Image obtained from Alicia Bentley's website.

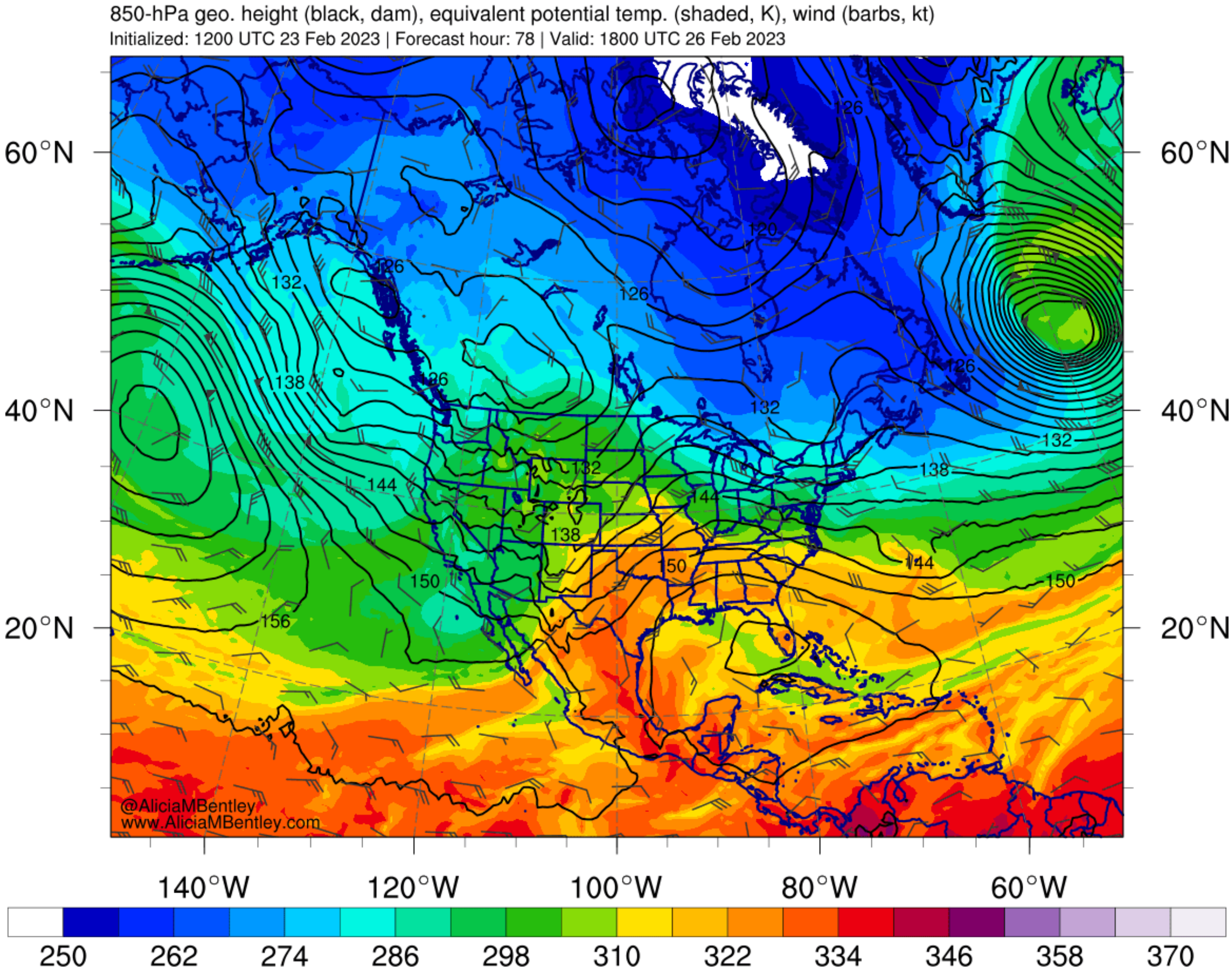

Figure 8: As in Fig. 7, except the 78-h forecast valid 1800 UTC 26 February 2023.

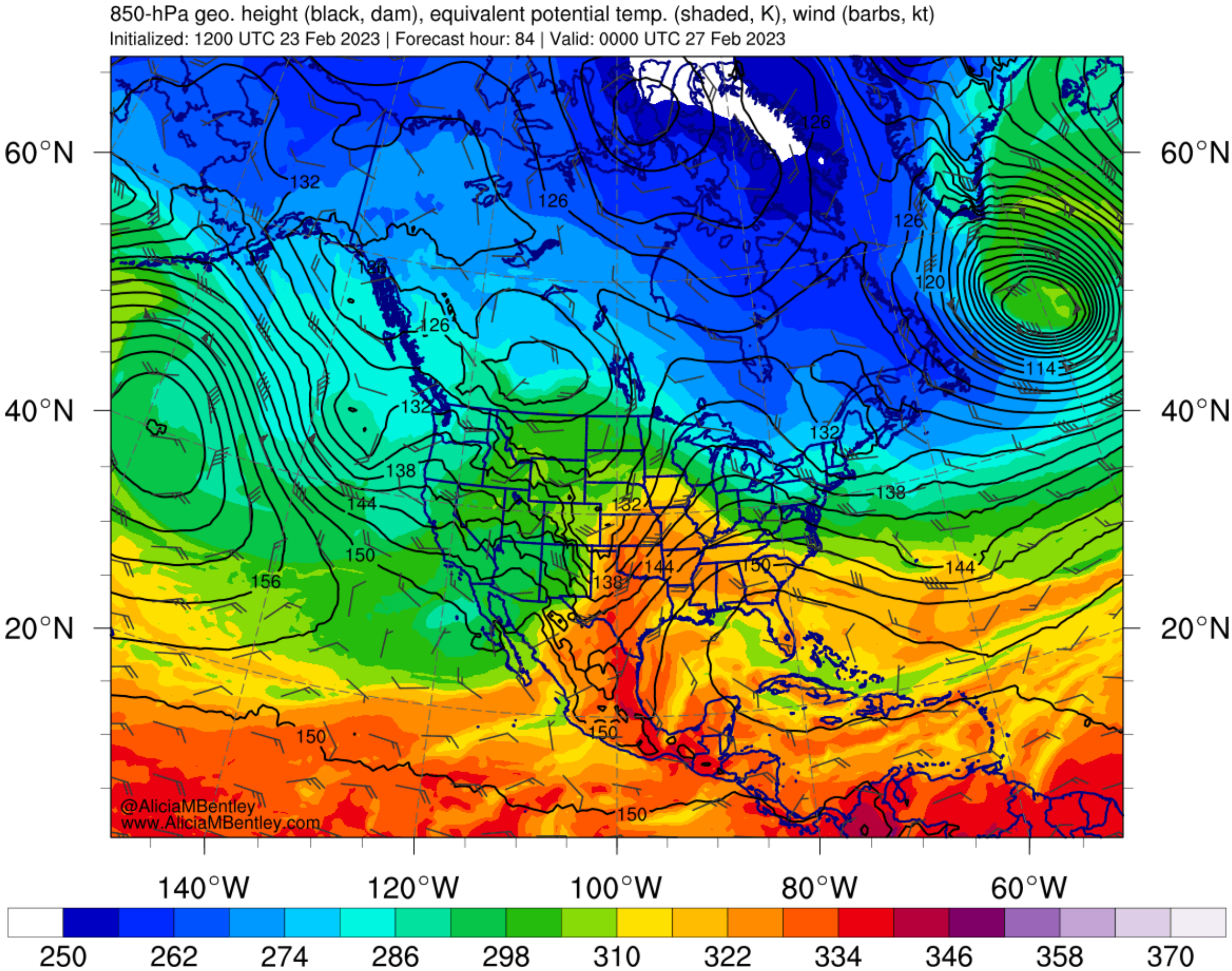

Figure 9: As in Fig. 7, except the 84-h forecast valid at 0000 UTC 27 February 2023.

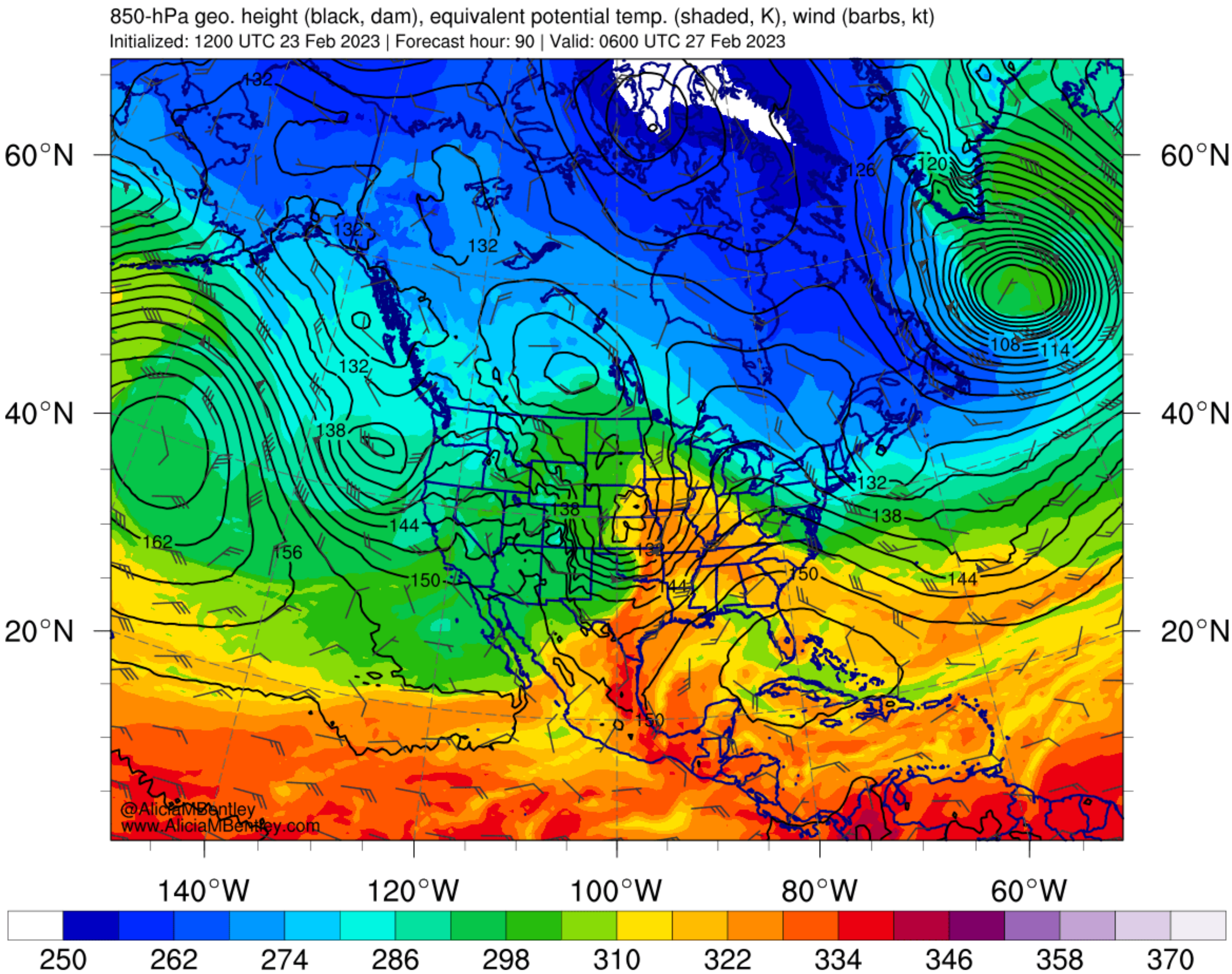

Figure 10: As in Fig. 7, except the 90-h forecast valid at 0600 UTC 27 February 2023.

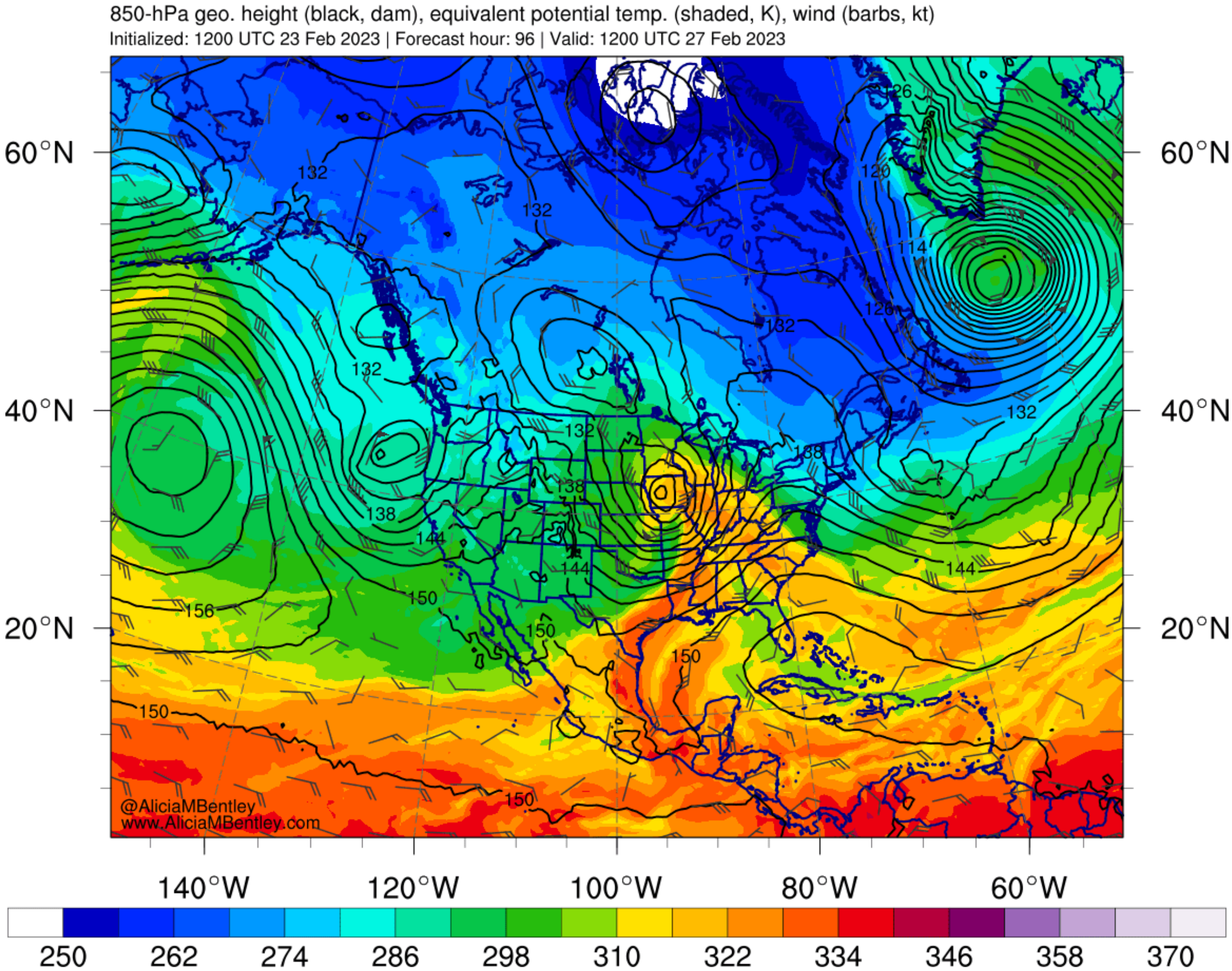

Figure 11: As in Fig. 7, except the 96-h forecast valid at 1200 UTC 27 February 2023.

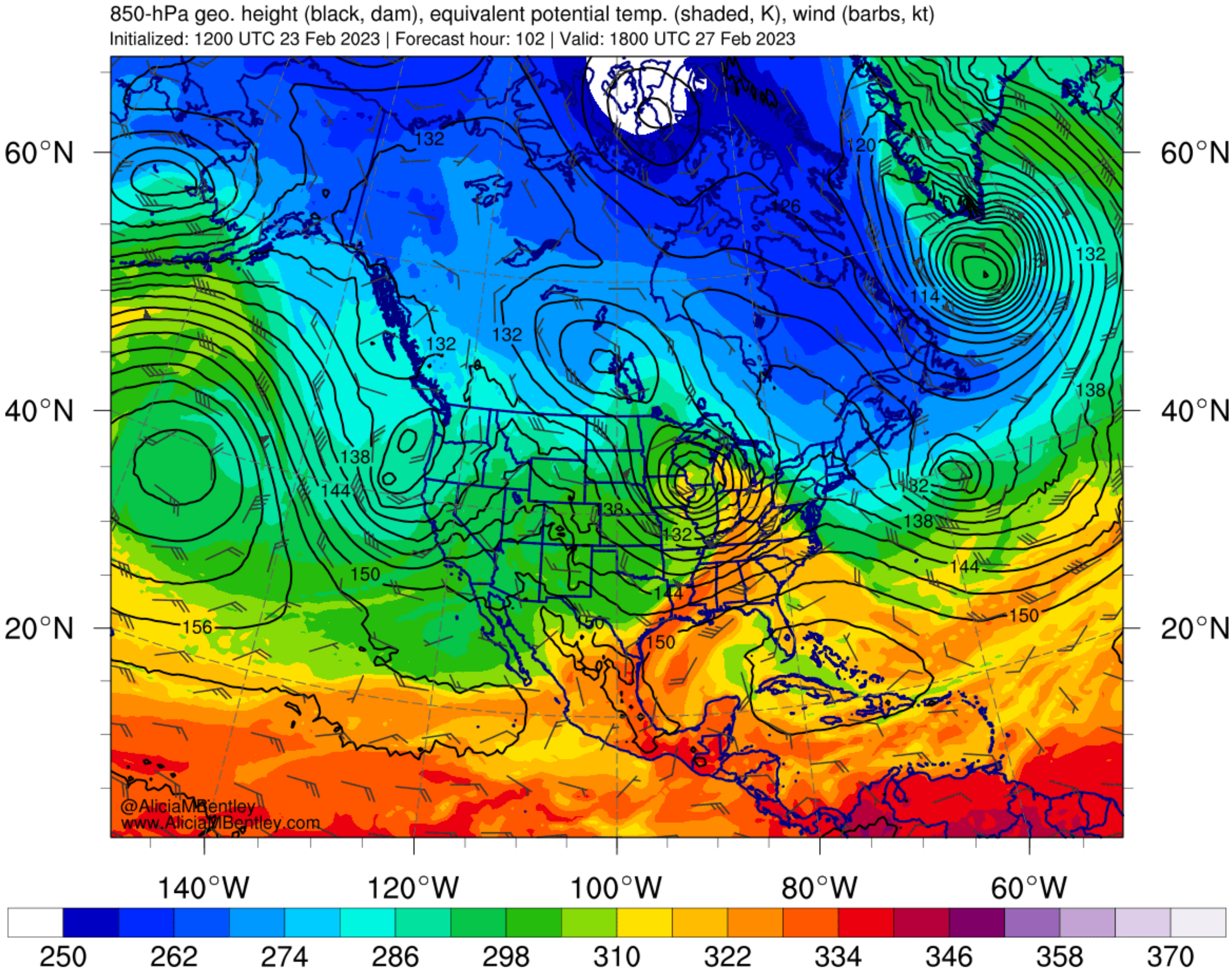

Figure 12: As in Fig. 7, except the 102-h forecast valid at 1800 UTC 27 February 2023.

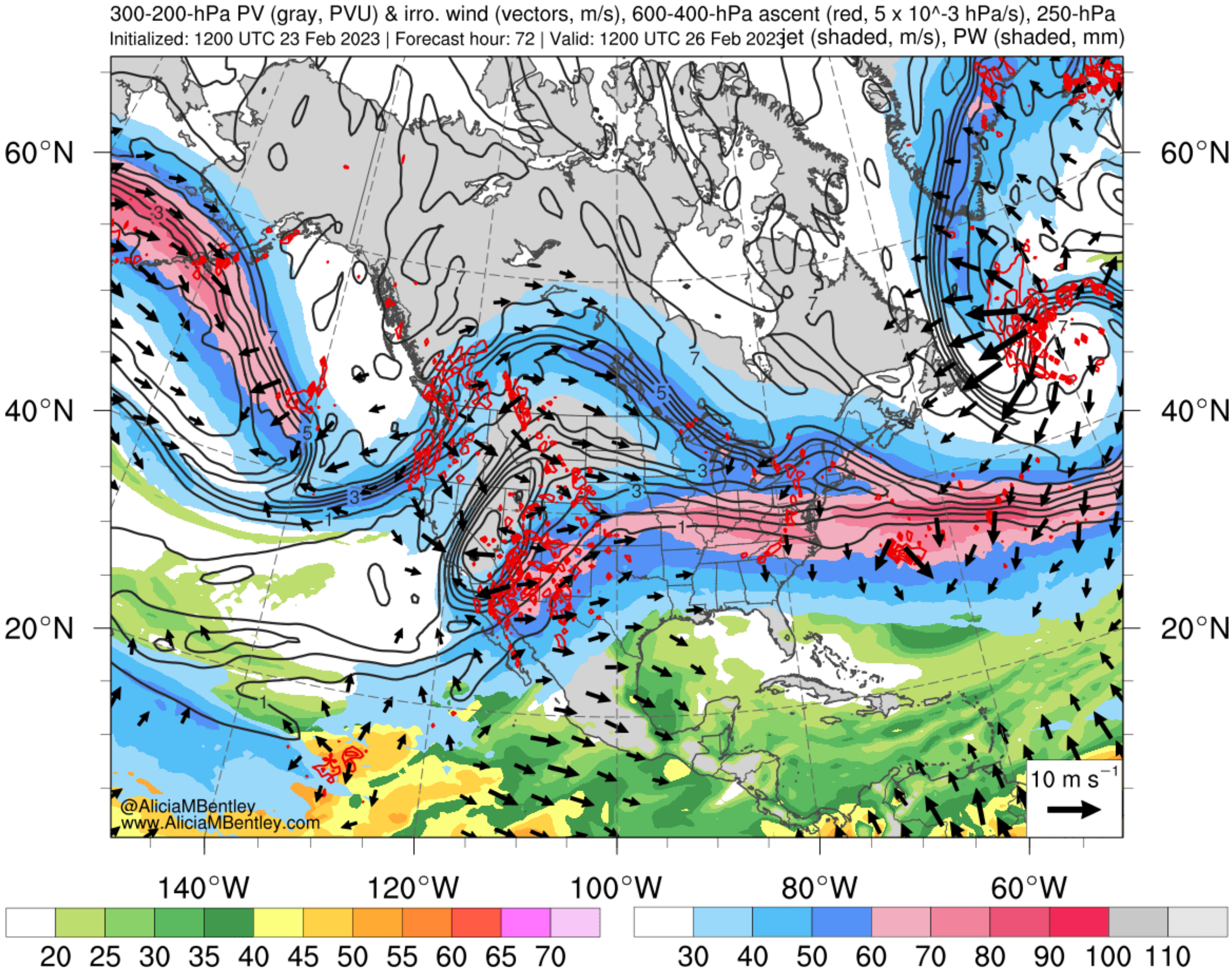

Figure 13: GFS 72-h forecast 300-200 hPa layer-mean potential vorticity (grey contours every 1 PVU), 300-200 hPa layer-mean divergent component of the wind (black vectors, with the reference vector given in the lower-right corner of each image), 600-400 hPa layer-mean ascent (red contours every $5x10^{-3}$ hPa s^{-1}), 250 hPa wind speed (shaded in cool colors in m s^{-1}), and column-integrated precipitable water (shaded in warm colors in mm). Image obtained from Alicia Bentley's website.

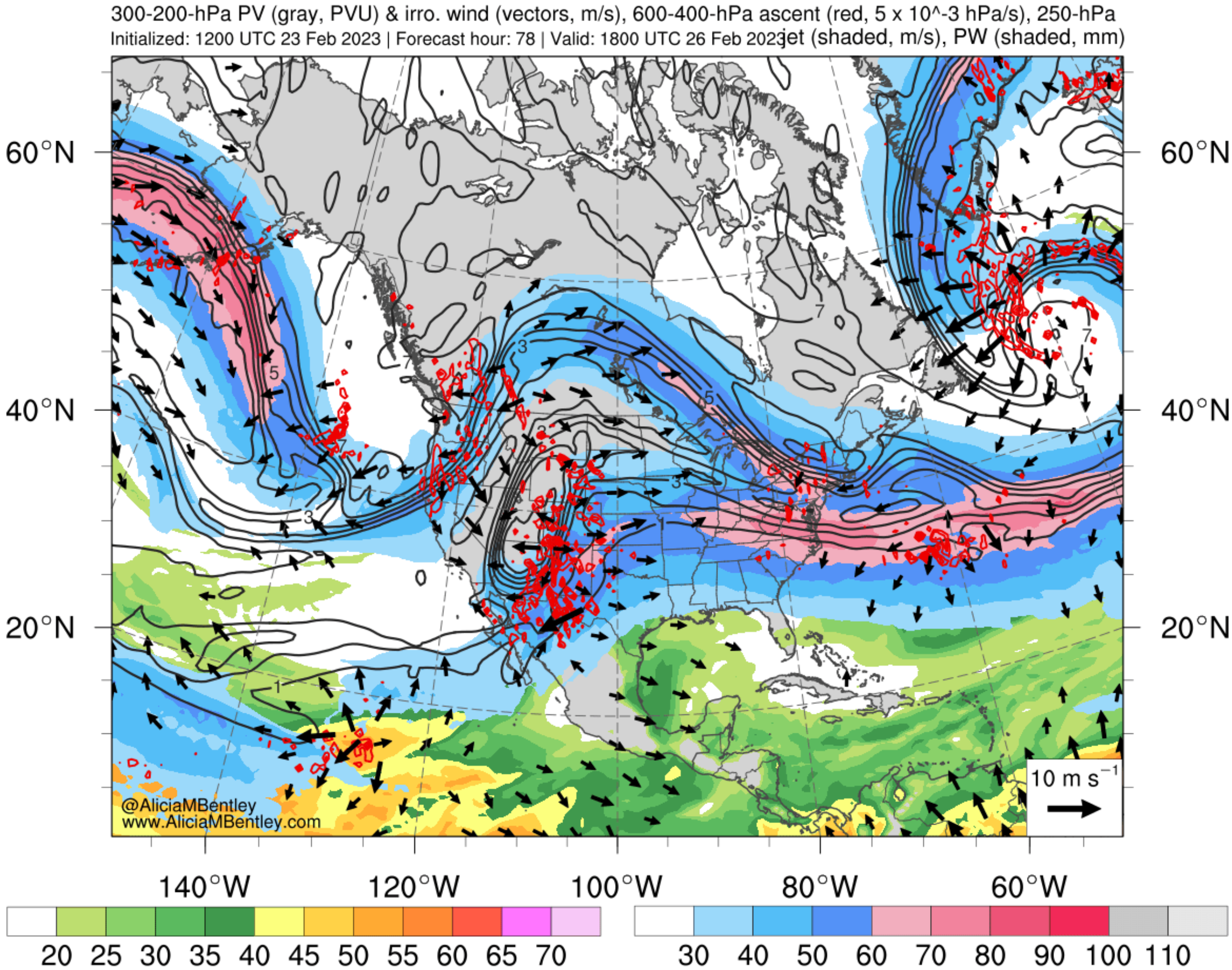

Figure 14: As in Fig. 13, except the 78-h forecast valid at 1800 UTC 26 February 2023.

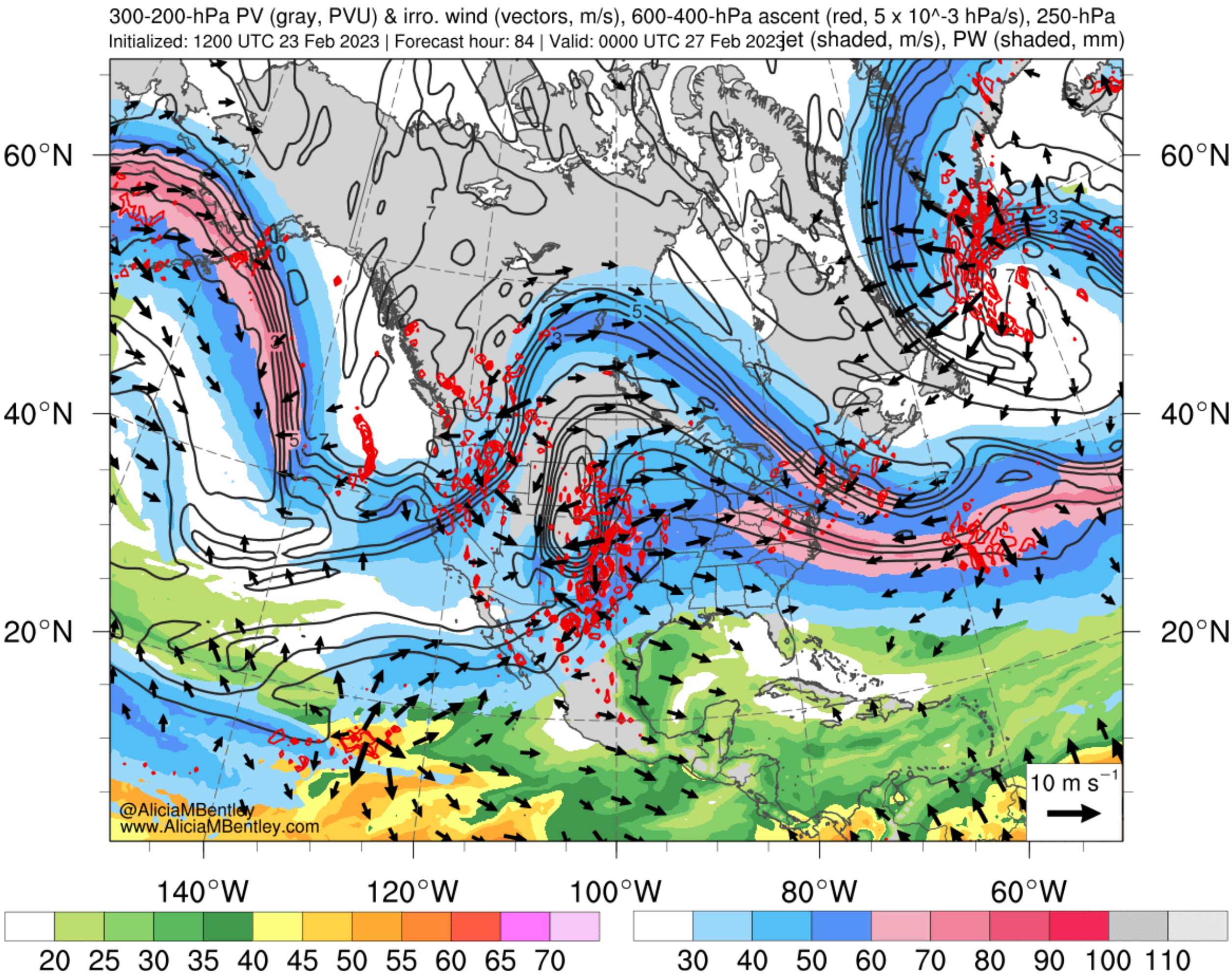

Figure 15: As in Fig. 13, except the 84-h forecast valid at 0000 UTC 27 February 2023.

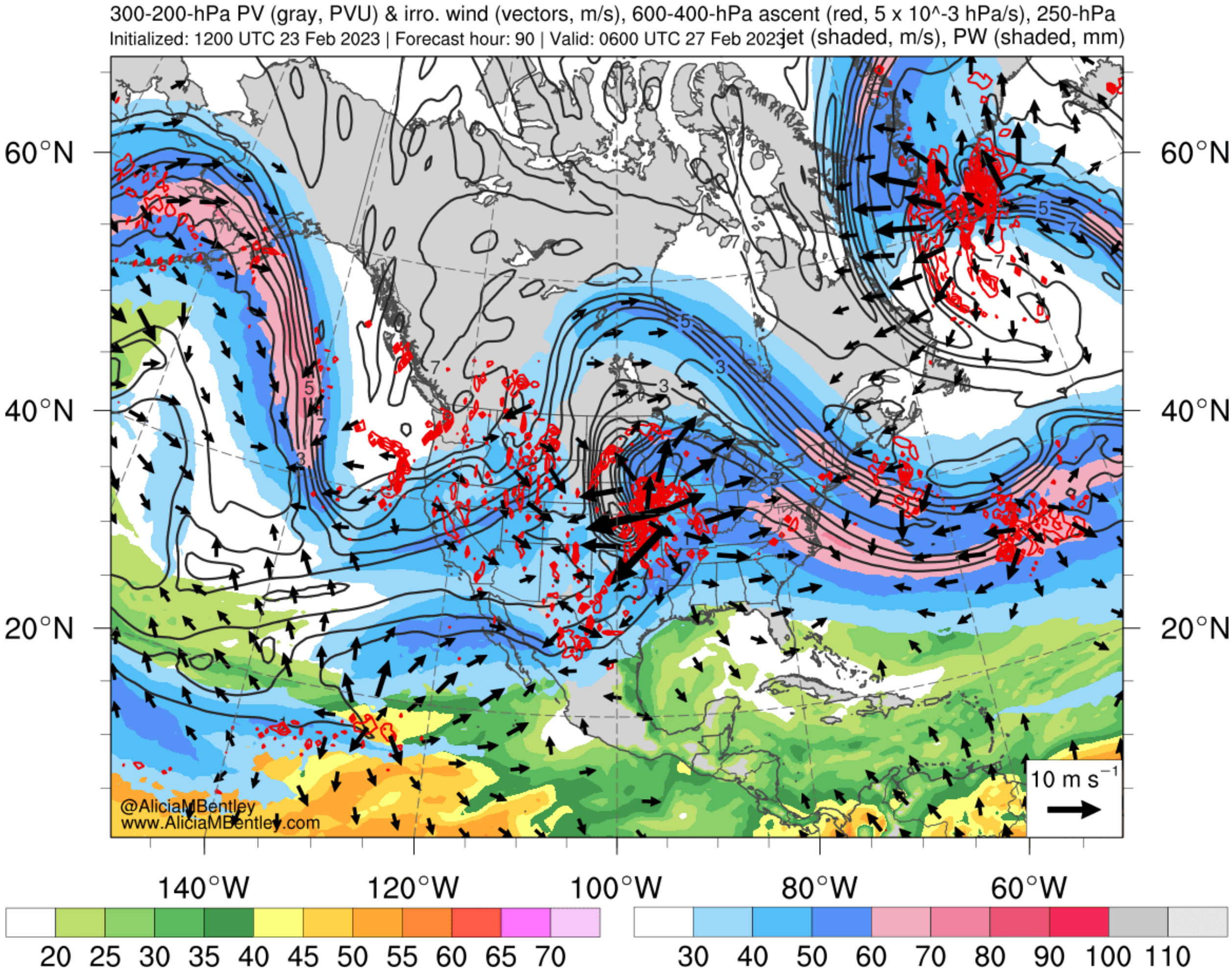

Figure 16: As in Fig. 13, except the 90-h forecast valid at 0600 UTC 27 February 2023.

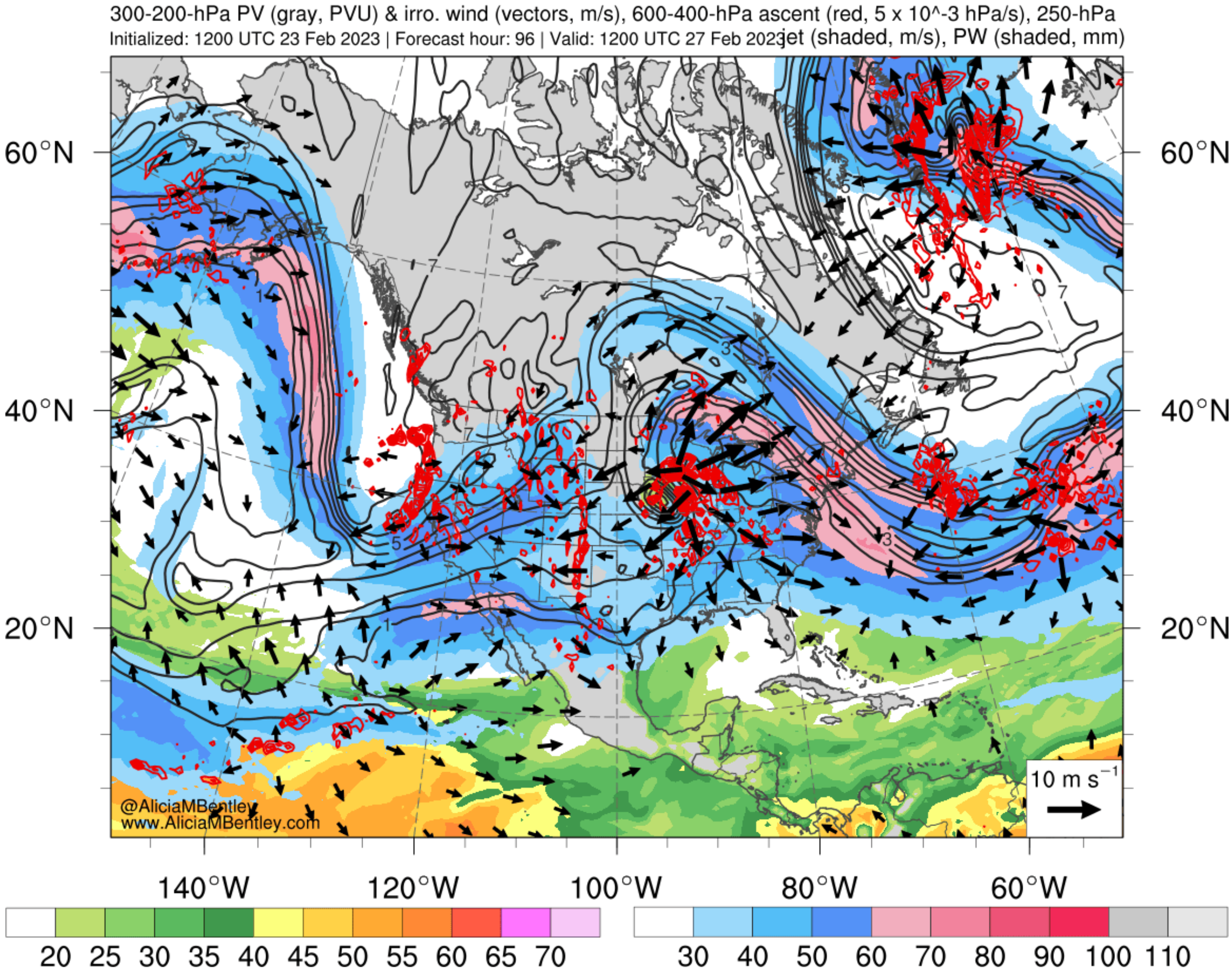

Figure 17: As in Fig. 13, except the 96-h forecast valid at 1200 UTC 27 February 2023.

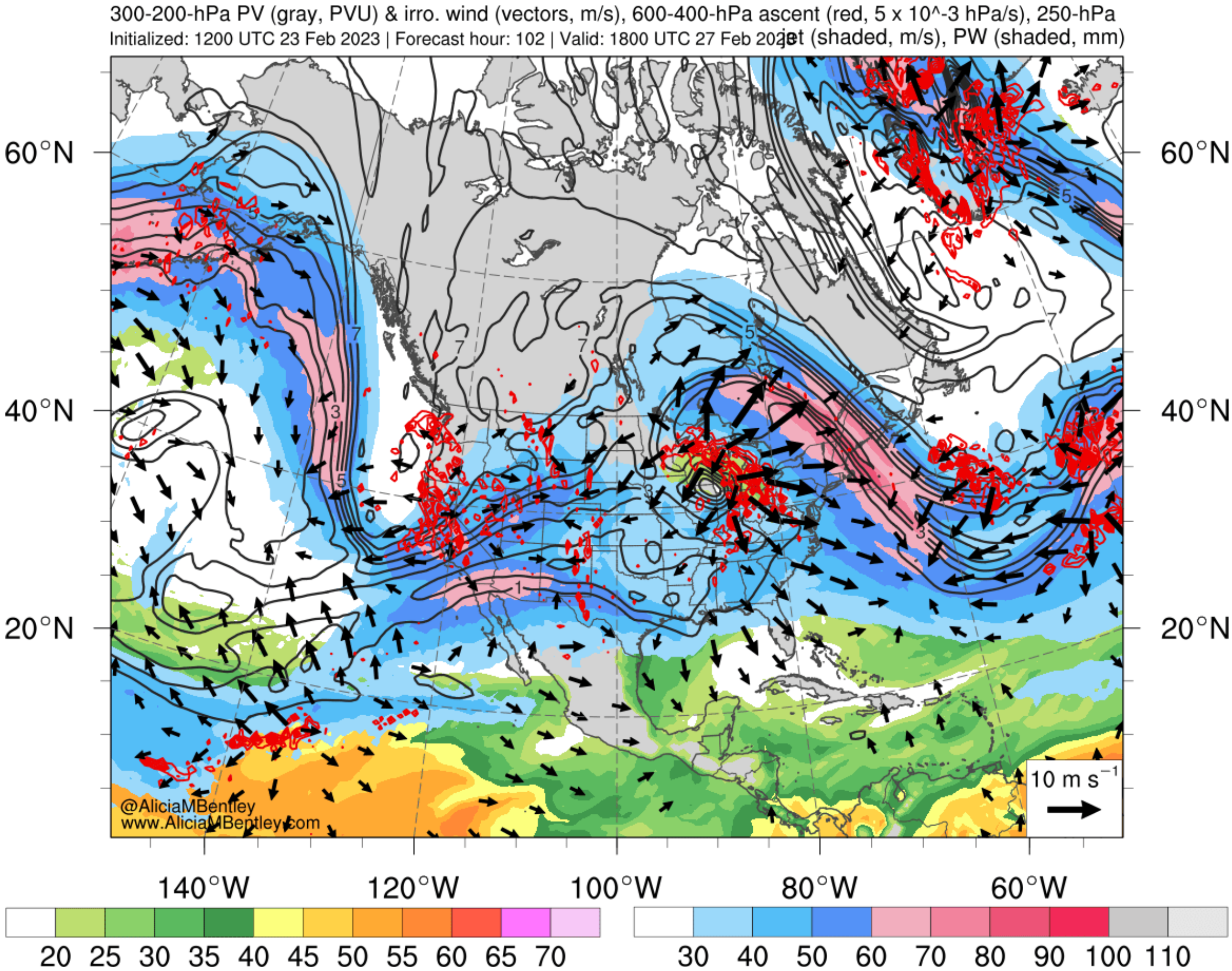

Figure 18: As in Fig. 13, except the 102-h forecast valid at 1800 UTC 27 February 2023.